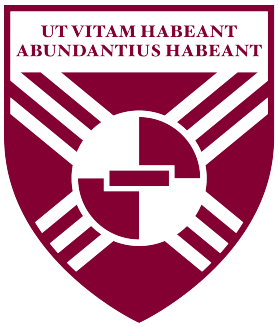

AMERICAN UNIVERSITY OF BEIRUT

MAROUN SEMAAN FACULTY OF ENGINEERING & ARCHITECTURE

Preliminary Design of a Go-Kart

Mohammad Shouman, Elias Sebaaly, Jawad Chamoun,
Roudy Hassan, Jad Dagher

Department of Mechanical Engineering

Summer 2025

MECH 420

Prof. Dr. Bassem El Zoghbi

Abstract

The proceeding article showcases the preliminary steps in the theoretical design of a go-kart. It begins at a presenting a main objective of traversing a predefined elliptic trajectory with constraints on maximum velocity. Based on an appropriate parametrization, analytical and numeric kinematic and dynamic analyses are performed to study the critical states of loading which the go-kart experiences. After reducing the dynamic problem into a static one, internal forces that accelerate and decelerate the axle are determined, reactions on bearing supports are computed, and shear-moment diagrams are drawn across the rear-axle. From then, standard fatigue and stress analysis tools are used to precise the critical points along the rear-axle and then compute the required diameter to support them. Checks are made to ensure that the factor of safety is met along the shaft. Afterwards, a minimal chassis design is tested using Finite Element Analysis. Bearings are selected to support the forces on the rear-axle, tolerances are computed, and a final full shop drawing is drawn.

Contents

List of Figures

List of Tables

Listings

1 Introduction

Go-karts are miniature, motorized vehicles built for racing and recreation. They consist, generally, of a chassis, engine, steering system, and a non differential rear-axle and they drive on four wheels with close proximity to the ground. Our goal is to design, build, and test a Go-kart that is capable of traversing an elliptical track, specifically, drive about the 'Green Oval' in the campus of the American University of Beirut, Lebanon, as seen in Figure 1, with a close focus on the rear-axle.

Figure 1: Green Oval

Using publicly available maps of the campus, including [1], we estimate the 'Green Oval' to be an ellipse with a major axis, which is the longest distance from the center of the ellipse to the boundary, of 30 meters, and a semi-major axis, which is the shortest distance from the center of the ellipse to its boundary, to be 12.5 meters. This allows for a dynamic model of the motion of the kart to be obtained, since the trajectory is well-defined, and for analysis based on analytical and numerical solutions.

Using said solutions, the points in time when the loading on the kart is maximal are precised, allowing for a static and fatigue stress analysis at the corresponding critical locations along the ellipse. Then, the rear axle dimensions can be found by applying an appropriate design criterion. Our choice of shaft-attachments on the rear-axle depend on the choice of engine which is a 6.5 horsepower diesel engine selected for its performance-to-cost ratio.

We utilize SolidWorks, a modeling and FEA (Finite-element analysis) tool, to create a virtual prototype of the kart, including shaft, chassis, wheels, bearings, disc brake, and sprocket. Stress and deflection analysis are also performed on the kart to verify safety before manufacturing.

Finally, the different kart components are to be built and assembled as per the SolidWorks model, and the kart is to be tested about the track at maximal loading conditions.

2 Literature Review

Unlike cars, buses, and other common automobiles, the Go-kart does not require or use a differential in its rear axle [2]. In a standard automobile, the differential serves to change the angular velocity of the rear wheels since the outer wheel always travels more distance than the inner when performing a turn or cornering. In stark contrast, the Go-kart uses a live axle, which is a shaft that connects the rear wheels and allows equal power transfer between them so that they rotate at an equal rate [3]. The reasons for this are lower cost and complexity, lower weight of the live axle allowing for greater speeds, and direct power transmission to the wheels which allows for greater acceleration at a fixed engine or motor power.

However, the simplicity of the design strips it of suspension, which is why a choice is made between a stiff or a soft rear axle [4]. A stiff axle can consist of a solid rod which has greater load bearing capacity while a soft axle can have a tube or pipe-like shaft that allows for greater flexibility. The loads considered vary from one study to another, but they include:

1. Chassis weight
2. Load capacity
3. Braking torque
4. Centripetal Tangential frictional force between tires and surface
5. Tangential frictional force between tires and surface

and more, which can occur during different phases of motion, like climbing, turning, accelerating, and breaking [5]. These produce different stresses, of which we highlight:

1. Normal stress due to bending moment due to weight shift of kart during accelerating, climbing, and turning.

2. Shear stress due to engine torque and braking.

Generally speaking, the analysis is static, which is done by fixing specific instances in time and finding shear and moment diagrams to compute the states of stress at critical points along the rear shaft [6]. The advantage of static analysis is the lack of necessity of simulation of the change in forces. However, fatigue analysis needs to be taken into account to account for component lifetime, especially the sprocket and bearings. Moreover, finite element analysis of the shaft under power take-off drive conditions shows strong agreement with analytical solutions [7]. FEA is best suited to find the safety factors while selecting different gears, motor mounts, and other drivetrain components before and after theoretical assessment of the final design. To simplify the dynamic analysis, In terms of material selection, AISI 1080 steel is an inexpensive yet effective option [4]. This, however, depends on budget constraints and local material availability.

Our modeling nevertheless simulates the kinematics and dynamics of the system over its period, but many simplifications are made. For instance, we assume that the forces on all four wheels are equal or that the weight is uniformly distributed on the wheels which is a common approximation in many dynamics problems. Without this assumption, each wheel would contribute three unknown reaction components (in the x, y, and z directions), leading to a total of 12 unknowns. Applying Newton's laws along with the equilibrium of moments about the three perpendicular axes provides only six independent equations. This under-determined system admits infinitely many solutions, forming a six-dimensional affine subspace of $\mathbb{R}^{12}$. Solving for the individual wheel forces in the general case would require more advanced techniques such as predictor-corrector methods and numerical simulations as seen in [8]. Such methods fall outside the scope of this course.

3 System Modeling

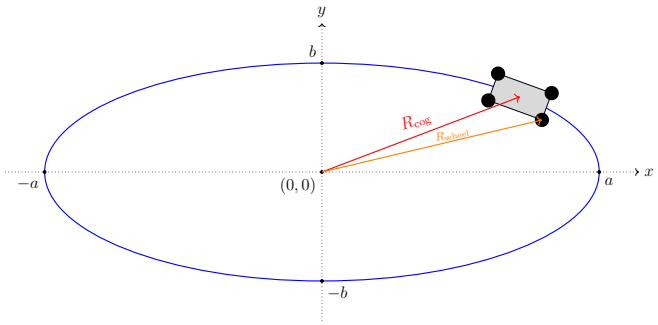

Figure 2: Simplified Model

3.1 Kinematics

The kart is modeled as a **rigid body** moving about an ellipse centered at the origin with major axis and minor axis of lengths $2a$ and $2b$ respectively. We define $\theta(t)$ as the parametrization function in time. Then, the parametric equations of position of the center of gravity of the kart are:

$$x = a\cos\theta(t)$$

$$y = b\sin\theta(t)$$

This pair satisfes the trajectory of the kart which is the equation of the ellipse:

$$\frac{x^2}{a^2} + \frac{y^2}{b^2} = 1$$

We assume that the kart takes a period of T to complete one revolution about the ellipse. The only constraints on the motion are that R_{cog} coincides with the abscissa at the start and end of the revolution. Assuming that motion starts at $t = 0$, this results in:

$$\theta(0) = 0$$

$$\theta(T) = 2\pi$$

meaning

$$\theta(t) = \frac{2\pi}{T}t$$

if we use a simple (polynomial) equation for theta. This can also be understood as a periodic motion with $\omega = \frac{2\pi}{T}$. Differentiating x and y in time, we obtain:

$$v_x = -a\dot{\theta}(t)\sin\theta(t)$$
$$v_y = b\dot{\theta}(t)\cos\theta(t)$$

We deduce the speed to be:

$$v = \sqrt{v_x^2 + v_y^2} = \dot{\theta}(t)\sqrt{a^2\sin^2\theta(t) + b^2\cos^2\theta(t)}$$

and the tangential acceleration:

$$a_t = \dot{\theta}(t)^2 \frac{(a^2 - b^2)\sin\theta(t)\cos\theta(t)}{\sqrt{a^2\sin^2\theta(t) + b^2\cos^2\theta(t)}}$$

since $\ddot{\theta}(t) = 0$. But $\theta(t)$ depends not only on time but also on the period, so the next step is to fix a value of T.

An appropriate choice of T is one that keeps the maximum speed within the range achieved by go-karts. For a very conservative upper bound, we choose T such that $v_{max} \approx 20$ m/s by a simple process of manual iteration, as the equations do not require a numerical solver. We obtain:

$$T = 3\pi \approx 9.42 \text{ s}$$

We also denote the radius of curvature of the ellipse at any instant by R, where [9]:

$$R = \frac{(a^2\sin^2(\frac{2}{3}t) + b^2\cos^2(\frac{2}{3}t))^{\frac{3}{2}}}{ab}$$

Moreover, the normal acceleration is:

$$a_n = \frac{v^2}{R}$$

Substituting $\theta(t)$, $\dot{\theta}(t) = \omega$, $T = 6\pi, a = 30$, and $b = 12.5$ into the above equations, we get the parametric equations that describe the motion of the center of gravity of the kart for $t \geq 0$:

- $x = 60\cos(\frac{2}{3}t)$
- $y = 25\sin(\frac{2}{3}t)$
- $v_x = -20\sin(\frac{2}{3}t)$
- $v_y = 8.3\cos(\frac{2}{3}t)$
- $v = 2\sqrt{100\sin^2(\frac{2}{3}t) + 17.4\cos^2(\frac{2}{3}t)}$
- $a_t = 110\frac{\sin(\frac{2}{3}t)\cos(\frac{2}{3}t)}{\sqrt{100\sin^2(\frac{2}{3}t)+17.4\cos^2(\frac{2}{3}t)}}$
- $a_n = \frac{55.6}{\sqrt{100\sin^2(\frac{2}{3}t)+17.4\cos^2(\frac{2}{3}t)}}$

3.2 Statics

The kart is designed in a symmetric manner such that the mass is uniformly distributed on the supports, i.e the wheels. Thus, the upwards reaction along the $\hat{z}$ direction is $\frac{Mg}{4}$ N on each wheel, where M is the total mass of the kart and driver. The rear axle is designed on the assumption that $M = 200$ kg, given the weight of the chassis, motor, attachments, and driver. We obtain:

$$N_{wheel} = 490.5 \text{ N}$$

per wheel.

3.3 Dynamics

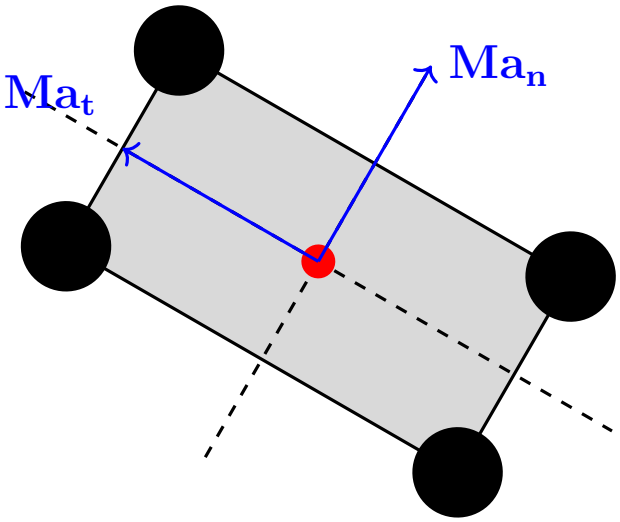

Figure 3: Forces on the COG

The center of gravity of the kart is assumed to lie in the xy plane alongside the centers of all the wheels. This is reflected in the design of the chassis which places the motor and rear-axle close to the ground. We study the forces along the normal and tangential directions at the COG as

shown in Figure 3. By Newton's Second Law, we have:

$$\sum (F_{ext})_t = Ma_t$$

$$\sum (F_{ext})_n = Ma_n$$

A few simplifying assumptions are made to reduce the computational complexity of the problem. First, we assume that the forces are **distributed equally** on all four wheels of the go-kart. Moreover, we use the fact that the kart is a **rigid body** whose **dimensions are much smaller** than those of the ellipse (about $1/10$) to neglect any changes in the accelerations between different points along the kart. This observation also allows us to model all points as moving on the **same elliptic trajectory** of dimensions (a, b)

We then move to analyze the forces on the rear wheels of the kart. The forces are frictional and are labeled f_t and f_n such that:

$$f_t = \frac{M}{4} a_t = 5500 \frac{\sin(\frac{2}{3}t)\cos(\frac{2}{3}t)}{\sqrt{100\sin^2(\frac{2}{3}t) + 17.4\cos^2(\frac{2}{3}t)}}$$

$$f_n = \frac{M}{4} a_n = \frac{2780}{\sqrt{100\sin^2(\frac{2}{3}t) + 17.4\cos^2(\frac{2}{3}t)}}$$

To ensure that no slipping occurs, the equivalent frictional force must be bounded by the coefficient of friction multiplied by the Normal force at the wheel:

$$f = \sqrt{f_n + f_t} < \mu_s N_{wheel}$$

The static friction coefficient for rubber on dry asphalt is approximately 0.9 [10]. So, we must have that:

$$\sqrt{f_n + f_t} < 441.5 \text{ N}$$

for all $t > 0$.

In order to verify the above condition and study the variation of the forces along the trajectory of the kart, we numerically compute values for position, velocity, forces, etc. using a simple MATLAB script, seen in Listing 1.

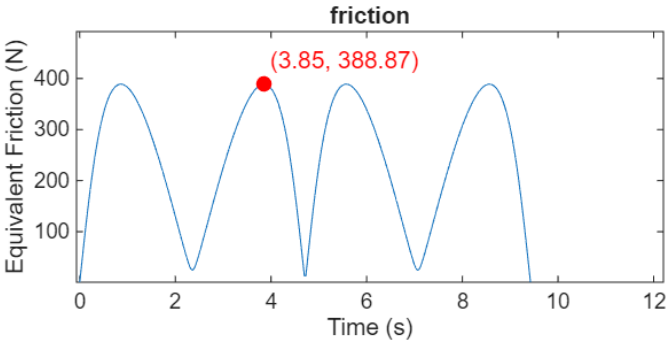

Figure 4: Equivalent Friction Plot

The maximum value of friction on any wheel is $f = 389$ N along the whole path, which is less than 441.5 N. Thus, no slipping between the wheels and the ground will occur at any time within our model.

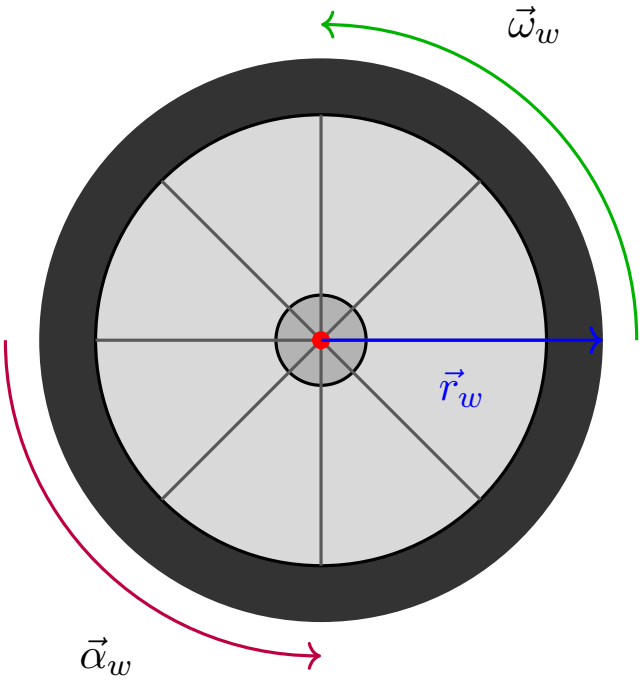

Figure 5: Rear Inner Wheel

We define ω_w to be the angular velocity of the wheel and α_w to be its angular acceleration. **We note that the wheel and the shaft have the same angular velocities and accelerations as they are concentric and rigidly attached**. Using the no-slip condition, we can write:

$$w_w r_w = v$$

and deduce

$$w_w = \frac{v}{r_w}$$

$$\alpha_w = \frac{a_t}{r_w}$$

with $r_w = 0.105$ m. The MATLAB script creates plots for these two quantities, renamed to describe the shaft, as shown:

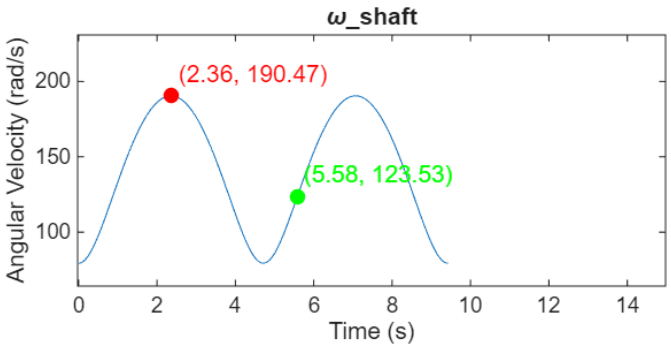

Figure 6: Angular Velocity of the Shaft

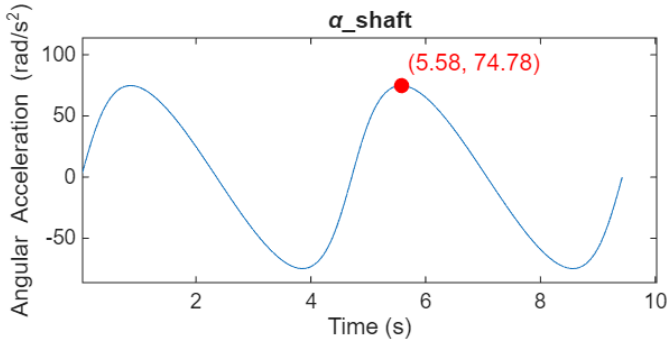

Figure 7: Angular Acceleration of the Shaft

```
a=30; b=12.5; M=200; r_wheel=0.105; T=3*pi; mu=0.9; omega=2*pi/T; t=
    linspace(0,T,300); theta=omega*t;
x=a*cos(theta); y=b*sin(theta); vx=-a*omega*sin(theta); vy=b*omega*cos(
    theta);
ax=-a*omega^2*cos(theta); ay=-b*omega^2*sin(theta);
v=sqrt(vx.^2+vy.^2); R=(x.^2+y.^2).^(3/2)./a*b; radius_ellipse=sqrt(x.^2+y
    .^2);
a_t=(omega^2)*(a^2-b^2).*sin(theta).*cos(theta)./sqrt((a^2)*sin(theta).^2+(
    b^2)*cos(theta).^2);
a_n=v.^2./R; a=sqrt(a_n.^2+a_t.^2); omega_shaft=v./r_wheel; alpha_shaft=a_t
    ./r_wheel;
f_n=M*a_n/4; f_t=M*a_t/4; friction=sqrt(f_n.^2+f_t.^2);

plot_with_max(t, friction, 'friction', 'Equivalent Friction (N)', 1);
plot_with_max(t, alpha_shaft, '\alpha\_shaft', 'Angular Acceleration (rad/s
    ^2)', 2);
plot_with_max(t, f_t, 'f_t', 'Tangential Force (N)', 4);
plot_with_max(t, f_n, 'f_n', 'Normal Force (N)', 5);
plot_with_max(t, radius_ellipse, 'radius of ellipse', 'Radius (m)', 6);
plot_with_max(t, omega_shaft, '\omega\_shaft', 'Angular Velocity (rad/s)',
    8);
plot_with_max(t, v, 'v', 'Velocity (m/s)', 9);

function plot_with_max(t, y, title_str, ylabel_str, idx)
    subplot(3,3,idx)
    plot(t, y)
    title(title_str)
    xlabel('Time (s)')
    ylabel(ylabel_str)
    hold on
    % Plot max
    [max_y, idx_max] = max(y);
    yrange = max(y) - min(y);
    plot(t(idx_max), max_y, 'ro', 'MarkerFaceColor', 'r')
    text(t(idx_max), max_y + 0.05 * yrange, sprintf(' (%.2f, %.2f)', t(
        idx_max), max_y), ...
        'Color', 'r', 'VerticalAlignment', 'bottom', 'HorizontalAlignment',
            'left')

    if idx == 8
        x0 = 5.58;
        y0 = interp1(t, y, x0);
        plot(x0, y0, 'go', 'MarkerFaceColor', 'g')
        text(x0, y0 + 0.05 * yrange, sprintf(' (%.2f, %.2f)', x0, y0), ...
            'Color', 'g', 'VerticalAlignment', 'bottom', '
               HorizontalAlignment', 'left')
    end
    hold off
end
```

Listing 1: MATLAB Script for Dynamic Analysis

4 Mechanical Design

4.1 Sprocket Design

The powertrain consists of the engine output shaft, a pair of sprockets, a chain, and the rear axle. In vehicle applications, sprockets and chains are a common, cheap, and effective way to transmit rotary power, as seen in bicycles and motorbikes.

The chosen engine has a rating of 3600 rpm. To increase the torque output, we choose a sprocket-chain system with a torque ratio of 3. Therefore, the output sprocket will rotate the rear-axle at 1200 rpm, which translates to around 125 rad/s.

The point highlighted in green in Figure 6 shows that this angular velocity is achieved at a time of 5.58 seconds, so this time is chosen for our static analysis. This point coincides with the maximum force and angular acceleration on the shaft; in fact, this was an **implicit constraint** within our dynamic analysis. Thus, at the critical location along the path of time 5.58 seconds, all our further static and fatigue analysis will be made.

We follow the procedure described in Machine Elements in Mechanical Design, Robert L. Mott et al., Sixth Edition, Chapter 7, Pages **281-286** to choose a proper chain-sprocket system [11]. From Table 7-14, we select a number of teeth for the counter-shaft (input) sprocket of:

$$N_1 = 12$$

and we conclude that the set needs a bath or disc lubrication upon installation. We also deduce the number of teeth of the rear (output) sprocket as:

$$N_2 = 35$$

since it's the nearest integer to $3 \times 12 = 36$ from Table 7-14. We can also conclude from the range of pitches in the table that the pitch is:

$$P = 0.5$$

We can then compute the pitch diameter [7-20] for the counter-shaft and rear sprockets, respectively:

$$PD_1 = \frac{P}{\sin\frac{180}{N_1}} = \frac{0.5}{\sin\frac{180}{12}} = 1.93 \text{ in}$$

$$PD_2 = 5.58 \text{ in} \approx 15 \text{ cm}$$

For the first iteration, we take the central distance, CD, to be 20 pitches. The required chain length is [7-18]:

$$\begin{aligned} L_c &= 2CD + \frac{N_2 + N_1}{2} + \frac{(N_2 - N_1)^2}{4\pi^2 CD} \\ &= 64.2 \text{ pitches} \end{aligned}$$

We deduce the real theoretical central distance by rounding L_c to 64 pitches and substituting into equation [7-19]:

$$\begin{aligned} CD &= \frac{1}{4}\left(L_c - \frac{N_1+N_2}{2} + \sqrt{\left(L_c - \frac{N_1+N_2}{2}\right)^2 - \frac{8(N_2-N_1)^2}{4\pi^2 CD}}\right) \\ &= 20.04 \text{ pitches} \end{aligned}$$

which translates to 10 inches.

Finally, we calculate the angle of the wrap for the counter-shaft and rear sprockets [7-21],[7-22]:

$$\begin{aligned} \theta_1 &= 180 - 2\arcsin\left(\frac{PD_2 - PD_1}{2CD}\right) \\ &= 159^\circ \\ \theta_2 &= 180 + 2\arcsin\left(\frac{PD_2 - PD_1}{2CD}\right) \\ &= 201^\circ \end{aligned}$$

which are acceptable values since they are greater than 120°.

Parameter	Value
Pitch	No. 40 chain, 0.5 in pitch
Chain Length	64 pitches
Center Distance (max)	10 in
Sprocket Spec	No. 60, 0.5 in pitch
Small Sprocket Teeth	12 teeth, PD = 1.93 in
Large Sprocket Teeth	35 teeth, PD = 5.58 in

Table 1: Summary of Sprocket-Chain Design

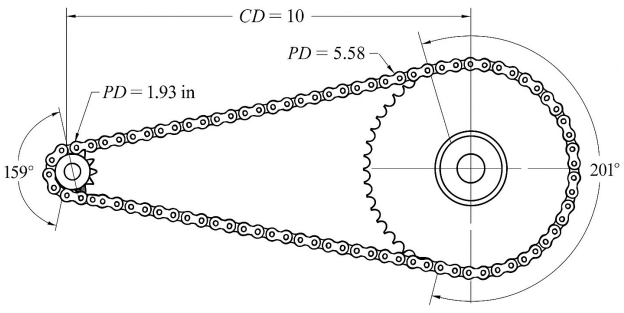

Figure 8: Chain-Sprocket Geometry

The pressure angle is found through the now-known geometry in Figure 8:

$$\theta_p = \arctan(\frac{1.8325}{10}) = 10.33°$$

4.2 Geometry and Stress Analysis

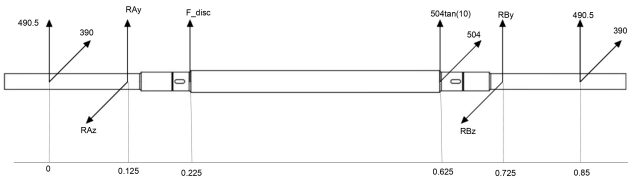

Figure 9: 3D Force Diagram

The power transmitted by the sprocket will be 98 % of that provided by the motor since the system is properly lubricated. Then, the torque is:

$$T = 0.98\frac{p}{w} = 38 \text{ Nm}$$

and the tangential force at the sprocket is:

$$F^z_{spr} = 2\frac{T}{pd_{sprocket}} = 504 \text{ N}$$

The angular acceleration at the instant is known through Figure 7, but the mass-moment of inertia of the shaft is unknown since it depends on the diameter of the shaft. For a very conservative estimate, we will take the diameter of the shaft to be 60 mm to compute the inertia, resulting in:

$$I\alpha = 0.75 \text{ Nm}$$

Moreover, the tangential forces and the normal reactions at the wheels are known. We wish to obtain the force applied on the disk upon breaking. Knowing that the effective diameter of the sprocket and disc brake is 15 cm and through summing the torques about the shaft by Newton's Second Law, we obtain:

$$\sum T_x = I\alpha$$

$$F^y_{disc} = 1586 \text{ N}$$

We can move on to find the reactions at the bearings. By a trivial application of the equations of forces and moments about the y and z, we find:

$$(R^y_A, R^z_A) = (-1828, 306) \text{ N}$$

$$(R^y_B, R^z_B) = (-829, -30) \text{ N}$$

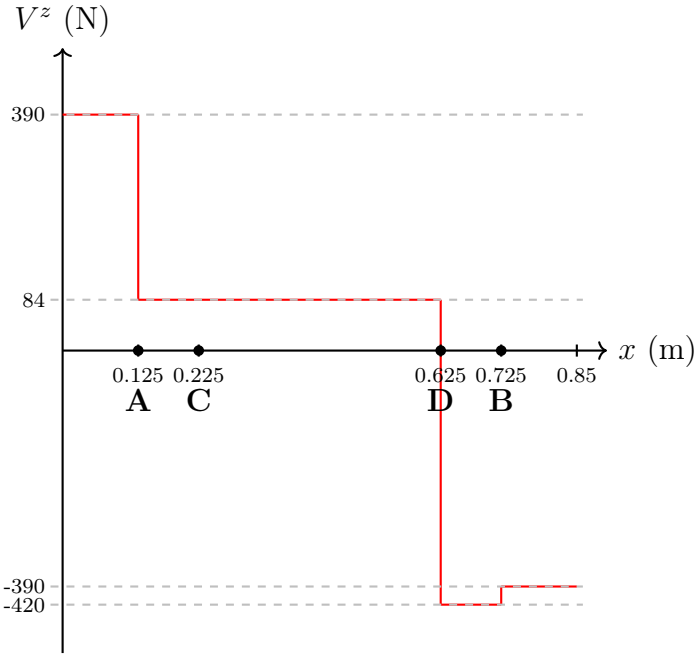

Figure 10: Shear Force Diagram in xz Plane

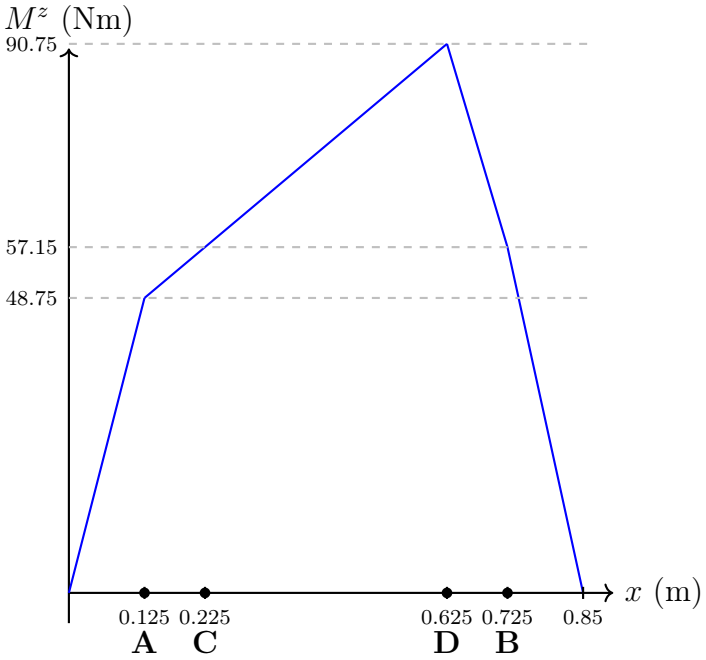

Figure 11: Bending Moment Diagram in xz Plane

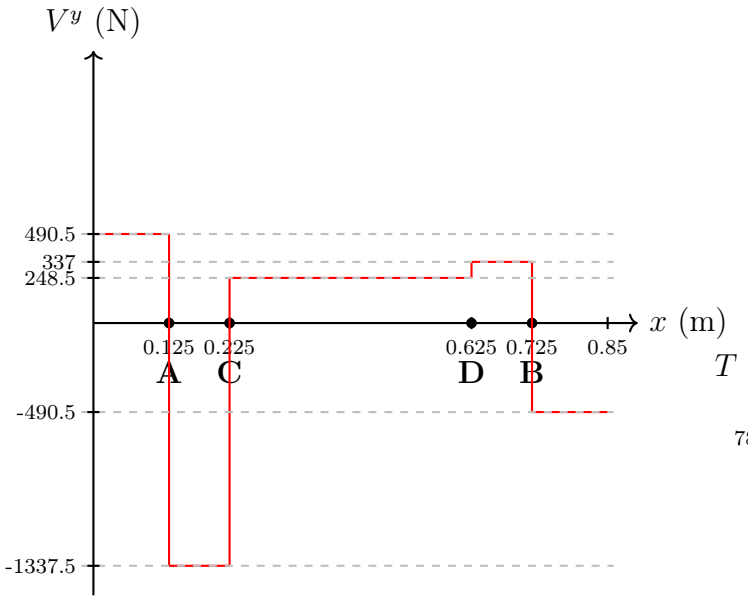

Figure 12: Shear Force Diagram in xy Plane

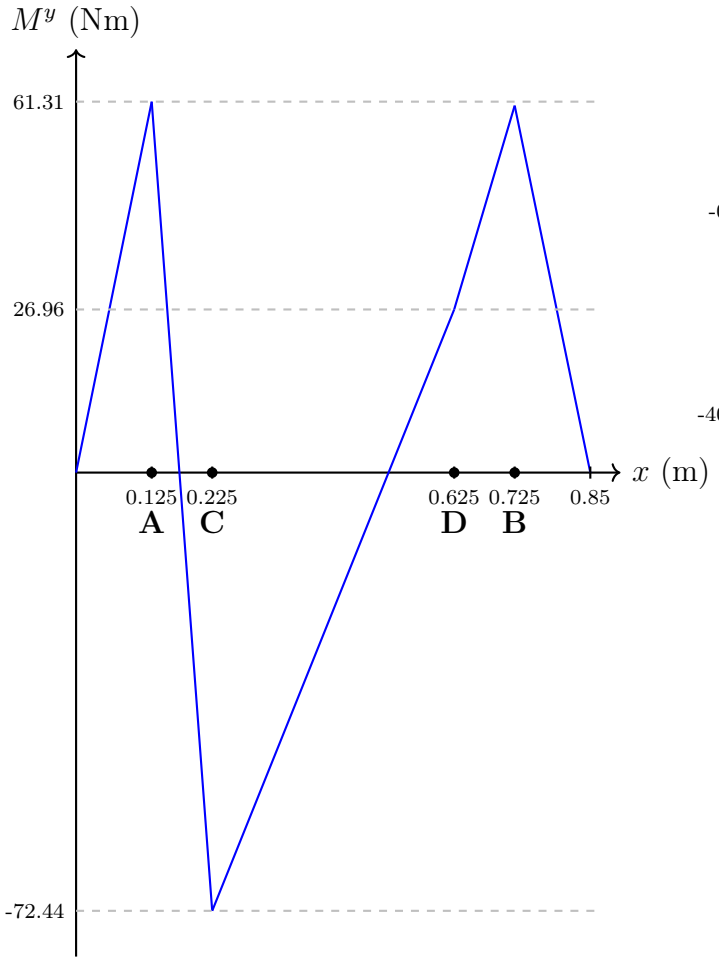

Figure 13: Bending Moment Diagram in xy Plane

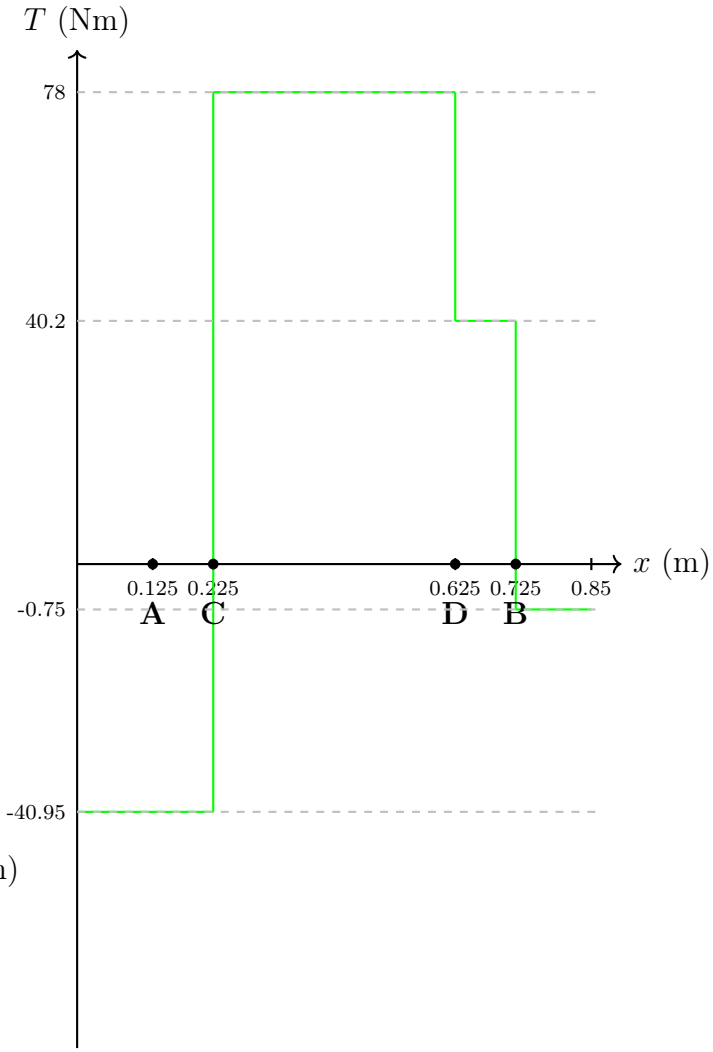

Figure 14: Torque Diagram

The maximum moments and torques occur at points C and D as seen in Figure 11, Figure 13, and Figure 14. We note that the torque just to the right of C is the same as that just to the left of D, and the torque to the left of C is the same as that to the right of D. Considering that these two locations share the same geometry, we take the location with greater bending moment as critical.

$$M_c = \sqrt{57.15^2 + 72.44^2} = 92.3 \text{ Nm}$$

$$M_D = \sqrt{90.75^2 + 26.96^2} = 94.7 \text{ Nm}$$

Practically, the locations at C and D are just as critical. Since D has a slightly higher bending moment, we will take it as the critical location for analysis. We identify the following sites on which we should compute the design factor of safety:

1. The shoulder between the largest and second largest diameters to the left of point D, subjected to M_D and $T = 78$ Nm
2. The shoulder between the second largest and smallest diameters to the right of point D, subject to M_D and $T = 40.2$ Nm
3. The key-seat to the right of point D, subject to M_D and $T = 40.2$ Nm
4. The groove to the right of point D, subject to M_D and $T = 40.2$ Nm

Our first choice of material is 1020 CD steel, with a yield strength of $S_y = 390$ MPa and an ultimate strength of $S_{ut} = 470$ MPa. The endurance can be calculated using:

$$Se = k_a k_b k_c k_d k_e Se' = 169.2 \text{ MPa}$$

with, as a first iteration:

$$k_c = k_d = k_e = 1$$

$$k_b = 0.9 \ (0.7 < k_b < 0.9)$$

$$k_a = aS_{ut}^b = 3.04(470)^{-0.217} = 0.8 \text{ (CD steel)}$$

$$Se' = 0.5S_{ut} = 235 \text{ MPa}$$

We will also take a standard shoulder ratio, using Table 7.1 [12]:

$$D/d = 1.2$$

for all shoulders along the rear-axle. Moving forwards, the largest, second largest, and smallest diameters are denoted D_3, D_2, and D_1 respectively.

To find a first iteration for the design diameter, we assume a sharp-fillet of ratio 0.02, and we calculate based on the first critical site, i.e the shoulder to the left of point D, using the conservative DE-Gerber criterion:

$$D_2 = \left(\frac{8nA}{\pi Se} \left(1 + \sqrt{1 + (\frac{2BSe}{AS_{ut}})^2} \right) \right)^{\frac{1}{3}} = 30.4 \text{ mm}$$

taking a minimum factor of safety $n = 1.7$,$K_f = 2.7$, and $K_{fs} = 2.2$. Since we have been conservative in our estimates, we take $D_2 = 30$ mm. Using the shoulder ratios:

$$D_3 = 1.2D_2 = 36 \text{ mm}, \ D_1 = \frac{D_2}{1.2} = 25 \text{ mm}$$

Taking $D_3 = 35$ mm to conform to standard values, we obtain the first iteration for the dimensions of the shaft. Now we calculate the real factor of safety at this critical site using a well rounded shoulder fillet ratio of 0.1. From Figures A-15-8 and A-15-9, we get:

$$K_t = 1.6, \ K_{ts} = 1.35$$

Thus, the corrected stress concentration factors are:

$$K_f = 1 + \frac{K_t - 1}{1 + \frac{\sqrt{a}}{\sqrt{r}}} = 1.47, \ K_{fs} = 1.23$$

with $\sqrt{a}$ being 0.493 for bending and 0.3711 for torsion and $r = 3$ mm.

Substituting into DE-Gerber, we get:

$$n_1 = 2.92$$

$$n_{y_1} = \frac{S_y}{\sigma'_{max}} = \frac{390}{83.43} = 4.67$$

We note the radius of fillet of the key-seat to be 0.6 mm, and the dimensions of the groove to be a width of 1.7272 mm, a depth of 1.2192 mm, and a corner radius of 0.254 mm. We repeat the process for each of the sites enumerated above, and summarize the results in Table 2.

Site	n	n_y
1	2.92	4.67
2	1.85	2.96
3	2.71	3.83
4	1.76	2.80

Table 2: Values of n and n_y at the critical sites

We conclude that the lowest factor of safety against failure by fatigue is 1.76 which occurs at the groove of the retaining ring. Since this is sufficient for our application, especially considering that we have been conservative in force analysis and choice of failure criterion, we deduce the final dimensions of the shaft as:

$$D_1 = 25 \text{ mm}$$
$$D_2 = 30 \text{ mm}$$
$$D_3 = 35 \text{ mm}$$

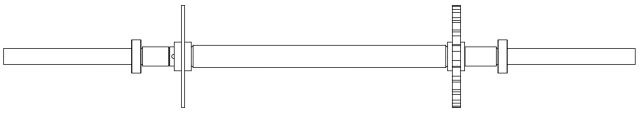

Figure 15: Shaft with Attachments

4.3 CAD Drawing and FEA

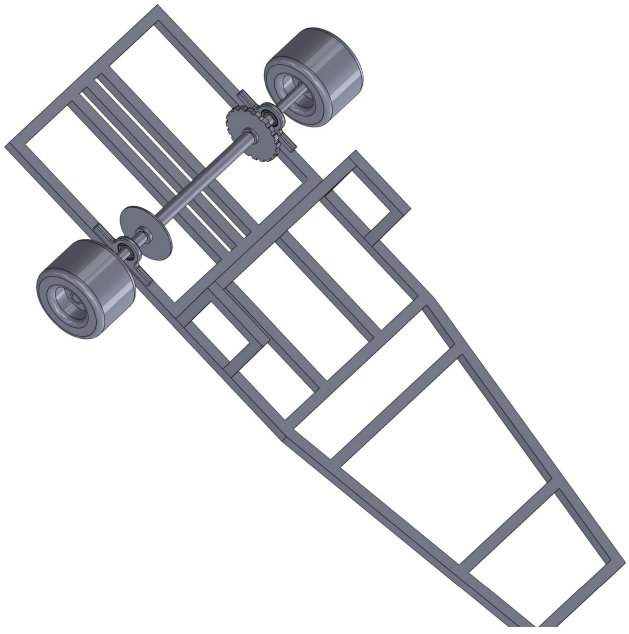

Figure 16: Chassis and Rear-axle Assembly

The chassis-rear axle assembly was completed using SOLIDWORKS as seen in Figure 16. The chassis was modeled based on a previous go-kart built at AUB with the goal of effectively carrying all the components while maintaining a uniform mass distribution to fit the dynamic analysis. The front wheels fit within a to-be-designed steering system based on an approximation of the Ackerman geometry approach. The sprocket and disk brake were modeled as per the prior dimensions, and the bearing CAD models were obtained directly from the SKF website after being selected in the next section of the report. Shoulders, keyseats, and grooves were all drawn using the theoretical dimensions utilized in the stress-analysis portion.

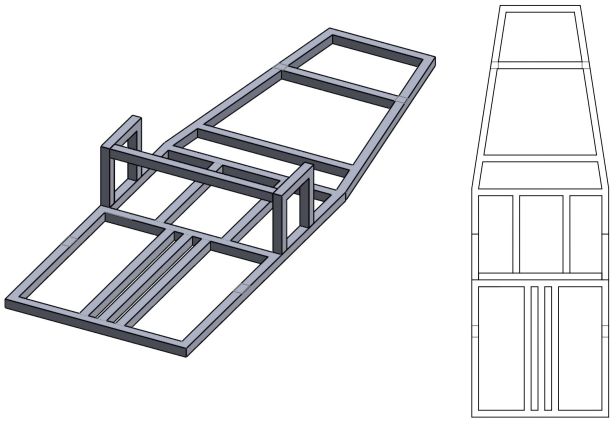

Figure 17: Chassis Geometry

The motor is supported by three metal rods in the back while the seat is supported by an extension as detailed in Figure 17. Welding was used to build the chassis from 30×30 mm, 2.5 mm thick metal rods for strength and cost effectiveness. This was verified by simulating the weighted loading on the chassis using FEA on SOLIDWORKS.

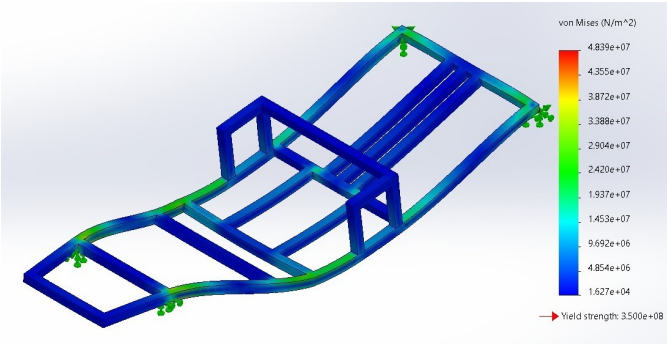

Figure 18: Stress Distribution on Chassis

The yield strength is 350 MPa meanwhile the maximum stress experienced at the middle corners of the chassis is around 50 MPa as seen in Figure 18. While this requires weld-stress analysis since it is the location of a welded corner between two rods, that is outside the scope of this course. It is experimentally known that this design holds up well for the relatively low loading of 200 kilograms on the chassis.

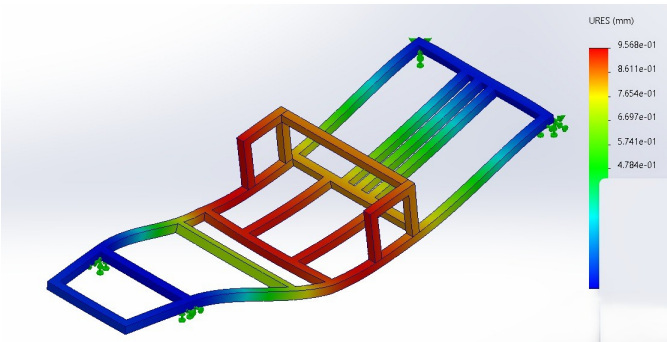

Figure 19: Deflection on Chassis

The deflection experienced on the metal frame is also minimal, having a maximum value of around 1 mm, well within the elastic range of the material. We conclude that the chassis is sufficiently strong to withstand the loading and use case of the go-kart, with further improvements depending on welding fatigue stress and deflection analysis.

5 Bearing Selection

Cylindrical roller bearings are used to effectively handle high radial loads, which occur at the bearing locations in our design. To select the correct bearings, we consider a maximum radial loading as prior and add to it the maximum axial force of:

$$F_a = 25 \text{ N} = 0.025 \text{ kN}$$

which is found via the MATLAB code in 3.3. Two bearings are required, one at point A and another at B. We aim at a reliability $R = 0.99$ per bearing and a lifetime of 5000 hours. We know the RPM to be 1200, and we take the application factor $a_f = 1.2$, noting that $V = 1$ for both bearings since the inner ring rotates. We begin by selecting the bearing at A. The equivalent radial force is:

$$F_R = \sqrt{(R_A^y)^2 + (R_A^z)^2} = 1853.45 \text{ N} \approx 1.85 \text{ kN}$$

Since both radial and axial forces are present, we begin iterating following the procedure developed in Example 11-7 [12] by selecting $Y_2 = 1.63$. Then:

$$F_e = 0.56F_R + 1.63F_a = 1.075 \text{ kN} < F_R$$

Since the equivalent force is less than the radial loading, we proceed using the radial loading as the design load, and we plug into equation 11-10:

$$\begin{aligned} C_{10} &\approx a_f F_D \left(\frac{x_D}{x_0 + (\theta - x_0)(1 - R_D)^{\frac{1}{b}}} \right)^{\frac{1}{a}} \\ &= 11.06 F_D \\ &= 20.5 \text{ kN} \end{aligned}$$

with $a = \frac{10}{3}$ for cylindrical bearings, $x_D = \frac{60 n_D \mathcal{L}_D}{10^6} = 360$, and Weibull parameters of $x_0 = 0.02$, $(\theta - x_0) = 4.439$, and $b = 1.483$. From Table 11-3, a 03-Series cylindrical roller bearing of bore 25 mm has $C_{10} = 28.6$ kN > 20.5 kN. It has a static load rating $C_0 = 15$ kN, so:

$$\frac{F_a}{C_0} = \frac{0.025}{15} \approx 0.00167$$

which is less than 0.014 in Table 11-9, whose value of e of 0.19. However:

$$\frac{F_a}{V F_R} = \frac{0.025}{1.85} = 0.0135 < e = 0.19$$

meaning that the axial load can be neglected. We deduce a choice of bearing to be a 25 mm bore

diameter, 52 mm outer diameter 03-Series SKF cylindrical roller bearing.

We move to selecting the bearing at B. The equivalent radial force is:

$$F'_R = \sqrt{(R_B^y)^2 + (R_B^z)^2} = 0.829 \text{ kN}$$

Via the same iterative procedure, we let $Y_2 = 1.63$ and find the equivalent force:

$$F_e = 0.56(0.829) + 1.63(0.025) = 0.505 \text{ kN} < F_R$$

Similarly, we proceed with F_R as the design load, and obtain:

$$C_{10} = 9.16 \text{ kN}$$

This C_{10} is lower than that at point A, as is expected since the overall load is lower. Moreover, the axial force is identical, so the same bearing can be chosen at B. As per the SKF website, the closest bearing currently available to the one selected is the 30205 single row tapered roller bearing [13], which boasts a C_{10} of 38.1 kN, far beyond our requirements. This bearing is thus selected.

6 Fits and Tolerances

The disc and sprocket have identical effective inner and outer diameters so tolerances are only needed for either of them. They also transmit torque primarily via the key and key-seat. Thus, the maximum torque due to their interference fit with the shaft is **neglected**. Therefore, we have little concern with special bore pressure requirements, but we need rigidity and alignment with a very high accuracy. We then choose a locational interference fit, specifically, H7/p6 from Table 7-9.

Using Table A-11, the shaft and hole dimensions (in mm) are found,

$$D_{min} = 30;\ \Delta D = 0.025;\ D_{max} = 30.025$$

$$\Delta d = 0.016;\ d_{max} = 30.042;\ d_{min} = 30.026$$

We deduce the maximum diametral interference from equation 7-43:

$$\delta_{max} = 0.042 \text{ mm}$$

Assuming that the shaft and hub are made from the same material, and using equation 7-40, the maximum interference pressure is:

$$p_{max} = \frac{E\delta_{max}}{2d^3}\left(\frac{(d_o^2 - d^2)(d^2 - d_i^2)}{d_o^2 - d_i^2}\right) = 137.8 \text{ MPa}$$

with $E = 205$ GPa, $d_o = 150$ mm, $d_i = 0$ mm, and $d = 30$ mm. The tangential stresses at the interface are, in MPa, by equations 7-44 till 7-47:

$$\sigma_{t,shaft} = 137.8;\ \sigma_{r,shaft} = -137.8$$

$$\sigma_{t,hub} = 149.24;\ \sigma_{r,hub} = -137.8$$

By applying the equation for the distortion energy theory in plane stress, the maximum equivalent stress can be found:

$$\sigma' = 248.6 \text{ MPa}$$

Finally, we compute the yielding factor of safety at the interface as:

$$n_y = \frac{390}{248.6} = 1.57$$

This is lower than the design factor of safety against failure by fatigue of 1.7, which signifies a need to reduce the interface pressure. This can be done by using a locational transition fit and by choosing smaller sprockets and disc brakes. However, due to the fact that the analysis has thus been rather conservative and to the fact that the shaft dimensions are standardized, allowing for these fits and tolerances is a low-risk compromise. Regular component maintenance is a key part of the common use-cases of go-karts, like in commercial racing tracks or personal recreational use.

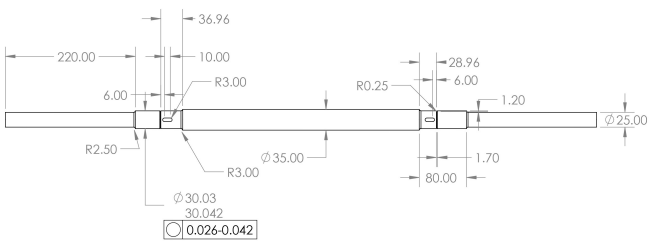

Figure 20: Shop Drawing

7 Improvements

An easy and relatively inexpensive way to improve the factor of safety is to use a higher strength steel, since at the given dimensions, a low amount is required for the rear-axle. Moreover, a more detailed exploration of the chassis factory of safety is needed, as previously mentioned, to care for the welds at the joints. The dynamic analysis can be more concise by using under-determined systems of forces and solving by predictor-corrector methods. Moreover, upon prototyping and testing, load cells, speedometers, and accelerometers can be placed around the kart to determine more accurately the force, velocity, and acceleration distributions on the kart.

Finite element analysis can be utilized to a much greater extent to measure the slopes and deflection at the shaft attachments. In addition, both static and dynamic numerical testing can be done using FEA to verify analytical results and even compute the factors of safety along every point on the rear axle. A dynamic version of the assembly, with steering and braking, would provide for a good insight on the kinematic testing without the need for constant physical measurements.

Finally, the same kart can be modeled for more extreme conditions, like higher engine power, slippery roads, greater weight capacity, and safer constraints on accelerations and decelerations.

8 Conclusion

This paper successfully accomplishes its goal of a preliminary design of a go-kart with a great focus on the rear-axle. It demonstrates learning objectives in MECH 420: Mechanical Design I by utilizing almost all the tools acquired throughout the semester. The go-kart will be built and tested on various conditions to verify the efficacy of the different estimates, approaches, and design decisions made by the authors. Finally, by drawing on more than a dozen references including two books on machine design, this paper represents the critical role of real-world applied education, which is the essence of engineering.

References

[1] American University of Beirut. Campus administrative building (cab). [Online]. Available: https://www.aub.edu.lb/facilities/fpdu/Documents/CampusBuildings/Campus%20Administrative%20Building%20(CAB).pdf

[2] "Why Go-Karts Don't Have a Differential | GoKartGuide — gokartguide.com," https://www.gokartguide.com/why-go-karts-dont-have-a-differential/.

[3] "What is a Live Axle on a Go-Kart? | GoKartGuide — gokartguide.com," https://www.gokartguide.com/what-is-a-live-axle/.

[4] S. Krishnamoorthi, L. Prabhu, M. Shadan, H. Raj, and N. Akram, "Design and analysis of electric go-kart," *Materials Today: Proceedings*, vol. 45, pp. 5997–6005, 2021, international Conference on Mechanical, Electronics and Computer Engineering 2020: Materials Science. [Online]. Available: https://www.sciencedirect.com/science/article/pii/S2214785320371297

[5] S. Singh, "Design and analysis of rear drive axle of go-kart," *IJSRD - International Journal for Scientific Research Development*, vol. 8, pp. 142–146, 11 2020.

[6] K. Mateja and K. Zenowicz, "Shaft design for electric go-kart," *Technical Sciences*, vol. 25, pp. 5–16, 02 2022.

[7] P. M. K. Khunti, "Stress analysis of shaft of pto drive using finite element analysis," *International Journal of Advance Engineering and Research Development (IJAERD)*, vol. 5, no. 4, p. 2535–2539, Apr. 2018. [Online]. Available: https://ijaerd.org/index.php/IJAERD/article/view/5098

[8] T. Mihalić, J. Hoster, V. Tudić, and T. Kralj, "Concept design and development of an electric go-kart chassis for undergraduate education in vehicle dynamics and stress applications," *Applied Sciences*, vol. 13, no. 20, 2023. [Online]. Available: https://www.mdpi.com/2076-3417/13/20/11312

[9] J. T. (https://math.stackexchange.com/users/48862/john tan), "Radius vs radius of curvature of an ellipse," Mathematics Stack Exchange, uRL:https://math.stackexchange.com/q/1159928 (version: 2018-08-04). [Online]. Available: https://math.stackexchange.com/q/1159928

[10] The Engineering ToolBox, "Friction - coefficients for common materials and surfaces," https://www.engineeringtoolbox.com/friction-coefficients-d_778.html, 2004, [Accessed 24 Jul. 2025].

[11] R. L. Mott, E. M. Vavrek, and J. Wang, *Machine elements in mechanical design*. New York: Pearson, 2018.

[12] R. Budynas and K. Nisbett, *Shigley's Mechanical Engineering Design*, 9th ed. McGraw-Hill, Jan 2008.

[13] 2025. [Online]. Available: https://www.skf.com/id/products/rolling-bearings/roller-bearings/tapered-roller-bearings/single-row-tapered-roller-bearings/productid-30205